Optimization of ionic conductivity in doped ceria

David A. Andersson*†, Sergei I. Simak‡, Natalia V. Skorodumova§, Igor A. Abrikosov‡, and Börje Johansson*§

*Applied Materials Physics, Department of Materials Science and Engineering, Royal Institute of Technology, SE-100 44 Stockholm, Sweden; ‡Department of Physics, Chemistry, and Biology (IFM), Linköping University, SE-581 83 Linköping, Sweden; and §Condensed Matter Theory Group, Department of Physics, Uppsala University, Box 530, SE-751 21 Uppsala, Sweden

Edited by Morrel H. Cohen, Rutgers, The State University of New Jersey, Piscataway, NJ, and approved December 22, 2005 (received for review November 2, 2005)

Oxides with the cubic fluorite structure, e.g., ceria (CeO_2), are known to be good solid electrolytes when they are doped with cations of lower valence than the host cations. The high ionic conductivity of doped ceria makes it an attractive electrolyte for solid oxide fuel cells, whose prospects as an environmentally friendly power source are very promising. In these electrolytes, the current is carried by oxygen ions that are transported by oxygen vacancies, present to compensate for the lower charge of the dopant cations. Ionic conductivity in ceria is closely related to oxygen-vacancy formation and migration properties. A clear physical picture of the connection between the choice of a dopant and the improvement of ionic conductivity in ceria is still lacking. Here we present a quantum-mechanical first-principles study of the influence of different trivalent impurities on these properties. Our results reveal a remarkable correspondence between vacancy properties at the atomic level and the macroscopic ionic conductivity. The key parameters comprise migration barriers for bulk diffusion and vacancy–dopant interactions, represented by association (binding) energies of vacancy–dopant clusters. The interactions can be divided into repulsive elastic and attractive electronic parts. In the optimal electrolyte, these parts should balance. This finding offers a simple and clear way to narrow the search for superior dopants and combinations of dopants. The ideal dopant should have an effective atomic number between 61 (Pm) and 62 (Sm), and we elaborate that combinations of Nd/Sm and Pr/Gd show enhanced ionic conductivity, as compared with that for each element separately.

density functional theory | diffusion | point defects | solid oxide fuel cells | CeO_2

Materials providing high conductivity of oxygen ions are urged by a number of important technological applications, such as oxygen sensors and solid oxide fuel cells (1). The latter are expected to become high-efficiency electrical power generators that enable clean energy production and support sustainable development (2–4). A standard electrolyte for solid oxide fuel cell applications is yttria-stabilized zirconia (YSZ) (1, 5). To increase the ionic conductivity of YSZ to a technologically useful level, high operating temperatures (≈1,000°C) are required. Lowering of the operating temperatures would considerably increase the applicability and competitiveness of solid oxide fuel cells. The ionic conductivity (σ) can be expressed as an exponential function of the activation energy for oxygen vacancy diffusion (E_a),

$$\sigma = \sigma_0/T \cdot \exp\left(-\frac{E_a}{k_B T}\right),$$

where T stands for temperature, k_B for the Boltzman constant, and σ_0 for a temperature-independent prefactor. Materials with lower E_a will facilitate ionic conductivity at lower temperatures, and here rare-earth doped ceria is one of the main candidates (1, 4). The basic principle for the choice of a dopant, advocated by many researchers, is the ability of the dopant to minimize the internal strain of the lattice (6–8). Clear understanding of the physics behind the ionic conductivity in doped ceria and the factors that determine E_a would be very helpful for future development of advanced solid oxide fuel cells.

For pure ceria, whose ionic conductivity is not particularly high because of low concentration of oxygen vacancies, E_a is equal to the sum of the vacancy formation energy (E_f) and the migration barrier (E_m). Ceria doped with lower valence cations contains intrinsic oxygen vacancies, which improve the conductivity. However, because of interactions, the dopants and vacancies form associates with a certain binding or association energy (E_{ass}), which prevents the vacancies from being mobile (9–12). The number of mobile vacancies is determined by E_{ass} in the same way as the concentration of vacancies in pure ceria is governed by E_f. Hence, for doped ceria, E_a can be identified as the sum of E_{ass} and E_m. At sufficiently high temperature, most vacancies will be dissociated, and in this regime, the concentration of mobile vacancies is simply determined by the doping level. However, in this article, we are interested in properties at low or intermediate temperatures. The aim is to maximize the concentration of mobile vacancies, which means that the dopant and dopant concentration should be chosen to minimize E_{ass}. In this strive, we focus on trivalent cations from the lanthanide series as well as Y^{3+}, which are widely used to dope ceria (5). Existing theoretical studies are either based on empirical atomistic models (12–14) or limited by too restrictive approximations, such as neglected relaxation of ionic subsystems (15). Quantum mechanical calculations within the density functional theory formalism can provide a unique understanding of atomic-level properties of fundamental importance in the search for improved ceria electrolytes. We have carried out such calculations by using the *ab initio* total-energy and molecular-dynamics program VASP (Vienna *ab initio* simulation program) (16, 17). We modeled defect properties within $2 \times 2 \times 2$ and $3 \times 2 \times 2$ supercells, derived from the ideal fluorite structure (Fig. 1*a*). Details about the calculations can be found in *Methods*.

Results and Discussion

First, we estimate how E_f, which is defined as the energy needed to remove an oxygen atom in the form of (half) an oxygen molecule from ceria that contains two trivalent ions that are situated next to each other, depends on the local configuration of vacancies and dopants. We have calculated E_f (Fig. 2) for the possible vacancy–dopant configurations in Fig. 1*b*. The negative vacancy formation energies are consistent with the fact that vacancies must form spontaneously if ceria contains trivalent ions. For Pm^{3+} and for ions to the right of Pm^{3+} in the lanthanide series, vacancies tend to occupy the nearest neighbor (NN) position, as measured from the dopants, whereas ions to the left of Pm^{3+} prefer to have vacancies in the next nearest neighbor (NNN) position. For Pm^{3+} E_f is almost independent of the exact

Conflict of interest statement: No conflicts declared.

This paper was submitted directly (Track II) to the PNAS office.

Abbreviations: NN, nearest neighbor; NNN, next nearest neighbor.

See Commentary on page 3497.

†To whom correspondence should be addressed. E-mail: davida@mse.kth.se.

www.pnas.org/cgi/doi/10.1073/pnas.0509537103

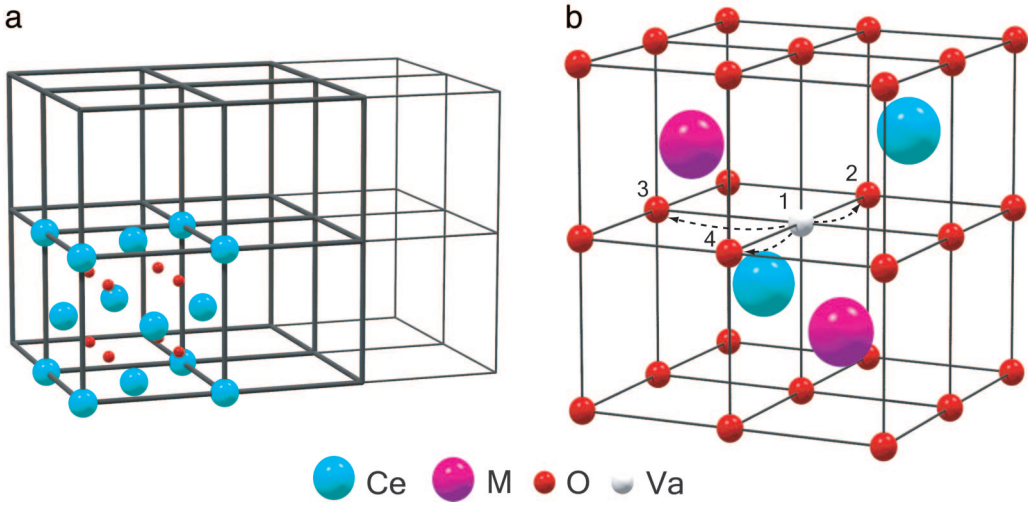

Fig. 1. The fluorite structure of ceria and the supercells used to study its defect properties. (*a*) The $2 \times 2 \times 2$ (96 sites) supercell of ceria (thick lines) and the $3 \times 2 \times 2$ (144 sites) supercell (thick and thin lines). For clarity atoms are only shown in one of the ceria unit cells. (*b*) A unit cell of ceria centered at the cubic oxygen sublattice. The cell contains two 3+ dopants (M) sitting next to each other and an oxygen vacancy. The numbers designate different locations that the vacancy can occupy with respect to the dopants, and the arrows schematically show how the vacancy can jump from site 1 to nearby sites, which is equivalent to oxygen diffusion in the opposite direction. Site 1 corresponds to the NN position, and site 2 corresponds to the NNN position. A vacancy moving from site 1 to site 2 is labeled as 1_2. Other diffusion paths are labeled correspondingly.

atomic level configuration, i.e., a crossover between NN and NNN preferences occurs. The same type of crossover occurs for vacancies in sites 1 and 3, however, except for the actual crossover point, E_f^3 always lies between E_f^1 and E_f^2. According to the relaxation pattern around vacancies, i.e., the NN distances, the volume available to the trivalent ions is larger for vacancies in the NNN position than in the NN position, which means that "small" ions prefer to have vacancies in the NN position and "large" ions prefer to have them in the NNN position. This finding relates the calculated site preference to the contraction of ions from left to right in the lanthanide series.

The four cations in the first coordination shell of a vacancy relax away from the vacancy, and because of symmetry, the relaxation pattern is split into two groups with two cations in each group. The relaxation distances are ≈0.13–0.19 Å. The six oxygens in the second coordination shell relax toward the vacancy according to a scheme with three symmetric groups, of which two groups contain one ion each and one group contains four ions. The maximum relaxation distances (≈0.20–0.40 Å) are larger than for the cations in the first coordination shell, although for most dopants (not for Ho^{3+} or Er^{3+}) the spread between different groups within the second coordination shell is larger than the corresponding spread in the first coordination shell. In particular, this is the case for vacancies in the NN position. The maximum relaxation distances within the second coordination shell are larger for vacancies that occupy the NNN position than for vacancies in the NN position. For vacancies in the NN position, the oxygen, situated closest to and symmetrically in between the trivalent ions, only relaxes very short distances. Beyond the second coordination shell, the relaxations are rather small. The relaxation patterns that we have calculated are consistent with recent extended x-ray absorption fine structure (EXAFS) and x-ray absorption near edge structure (XANES) spectroscopy measurements, which show that upon doping with trivalent ions, the Ce—O interatomic distances decrease (18). In agreement with experiments, we also predict the size of this decrease to be smaller for an increasing atomic number of the lanthanide elements (18).

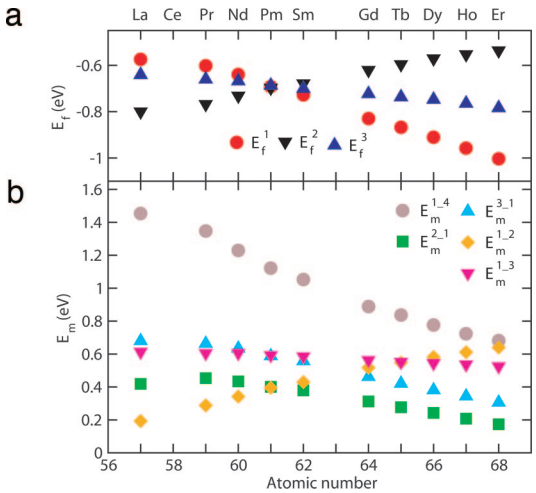

Fig. 2. Defect formation (*a*) and migration parameters (*b*) obtained for NN 3+ dopants in the $2 \times 2 \times 2$ supercell. The superscripts of E_f and E_m refer to the labeling in Fig. 1*b*.

The site preference of vacancies is determined by the strength and nature of the interaction with the trivalent dopants, which can be divided into elastic and electronic parts (19). The elastic part is mediated by lattice deformations and the electronic part by redistribution of the electronic structure. Because vacancies and trivalent dopants have effective charges of different signs, they will attract each other. All vacancy–dopant interactions vanish if the trivalent ions and the vacancy are sufficiently far away from each other. This situation can be modeled by separating the vacancy from the trivalent ions in our supercell. The electronic interactions can be evaluated by calculating the unrelaxed energy difference between a supercell with a vacancy in the NN or NNN position and a supercell where the trivalent ions and the vacancy are separated (Fig. 3). An unrelaxed supercell implies that the atoms are kept in the original fluorite positions. The same energy difference for relaxed supercells includes both elastic and electronic interactions. Consequently, it is possible to extract the elastic interactions by subtracting the electronic interactions from the total interactions (Fig. 3). As expected from electrostatics, the electronic interactions are strongest in

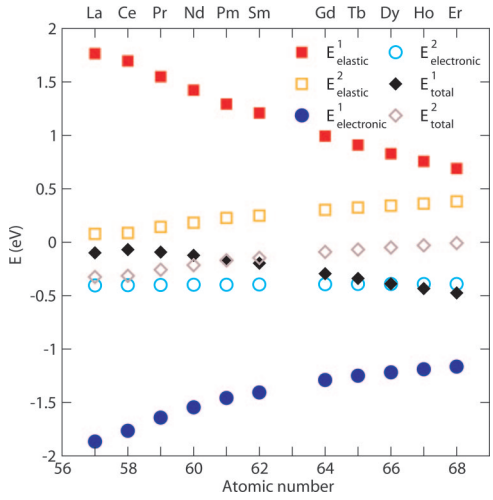

Fig. 3. Total, electronic, and elastic vacancy–dopant interactions as calculated for NN 3+ dopants in the 2 × 2 × 2 supercell. The superscripts refer to the labeling in Fig. 1*b*.

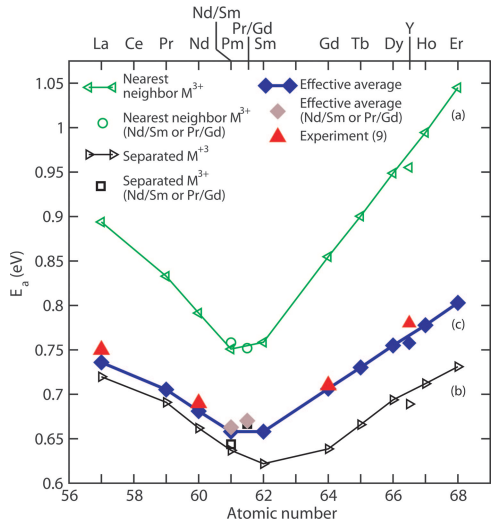

Fig. 4. E_a for dopants sitting next to each other (*a*) and separated from each other (*b*) and an effective average of the former two (*c*) (see text). The results were obtained within the 3 × 2 × 2 supercell, which implies a dopant concentration of 4.2%. The experimental values refer to the same doping level (9). Nd/Sm and Pr/Gd represent a mixture of 3+ dopants and have been placed according to their average atomic numbers. Because of its similarities with Dy and Ho, Y has been inserted at an effective atomic number of 66.5 (21).

the NN position (the negative numbers imply attractive interactions), and they decrease as we move from left to right in the lanthanide series. Because of the effective screening and larger separation of dopants and vacancies, the electronic interactions are much weaker in the NNN position. The NN elastic interactions are highly positive for dopants in the beginning of the lanthanide series and then decrease quickly as the atomic number increases. They are much stronger than the elastic interactions in the NNN position, and, additionally, the latter increase as a function of the atomic number. The decrease of the elastic interactions (positive) is faster than the decrease of the attractive electronic interactions. The decisive factor seen by nature is, of course, the total interactions. Therefore, from Fig. 3 we conclude that it is the balance between elastic and electronic contributions that determines the NN or NNN site preference. Naturally, for each dopant, the ground-state corresponds to the most negative of the total interactions. Remarkably, for the atomic number close to 61, the elastic and electronic interactions are balanced in such a way that the total interactions in the NN and NNN positions are almost identical.

E_m depends on the local atomic arrangement. If there are no trivalent ions around a vacancy, E_m is 0.46 eV. This value corresponds to the diffusion of oxygen ions far away from any dopants. We have calculated a subset of E_m for oxygen diffusion in the neighborhood of the NN trivalent dopants (Fig. 2). $E_m^{1\text{–}2}$ or $E_m^{2\text{–}1}$ always provides the lowest barrier and $E_m^{1\text{–}4}$ provides the highest, which is explained by the fact that it is less favorable for the oxygen atom to move through a saddle point close to large trivalent ions than to move close to smaller Ce^{4+} ions. $E_m^{1\text{–}3}$, $E_m^{3\text{–}1}$, and $E_m^{1\text{–}4}$ all decrease for increasing atomic number of the lanthanide dopant, which is straightforwardly connected to the contraction of ions along the lanthanide series. The slope of $E_m^{1\text{–}2}$ and $E_m^{2\text{–}1}$ in Fig. 2 is determined by the preference of vacancies to occupy the NN or NNN position, i.e., the balance between elastic and electronic vacancy–dopant interactions. As for the vacancy formation energies, we notice a crossover for the migration barriers close to Pm^{3+}. For increasing doping concentrations, vacancies, on average, will experience more trivalent dopants in their immediate neighborhood. As a result, the number of low barrier migration paths decreases, which at sufficiently high doping concentrations must limit the ionic conductivity (20).

E_a can be calculated as the sum of E_{ass} and E_m for bulk diffusion (≈0.5 eV). The value of E_{ass} depends on the distribution and concentration of 3+ ions. In the present study, we considered two limiting cases: (*i*) NN 3+ ions and (*ii*) separated 3+ ions. From Fig. 4, we conclude that case *i* always corresponds to the highest E_{ass}. Thermodynamically the defects of type *i* are the most stable configurations. Our calculations show that the binding energies for trivalent dopants range from 0.02 eV for Pm^{3+} to 0.23 eV for Er^{3+}. The binding energy as a function of the atomic number has a clear minimum close to Pm^{3+} (data not shown). Because of slow cationic diffusion, the equilibrium distribution of dopants on the cationic sublattice may not be reached; nevertheless, high binding energies should yield an excess number of dopant clusters compared to the completely random distribution of cations. In experimental investigations, one generally assumes that only defects of type *ii* are present, and consequently just one effective value of E_a is calculated. Thus, the measured E_a should lie between the two limiting cases. We would like to estimate this value. For the present dopant concentration range (≈4.2%), we accomplish this by calculating an effective association energy, resulting from the presence of dopants in both type *i* and type *ii* configurations. The fraction of dopants in each configuration can be estimated by treating the dopants as randomly distributed. A standard system of mass action equations (22) connecting two types of the vacancy equilibria (11), one for the 3+ dopants being NNs and the other for the separated 3+ dopants, has been solved to extract effective E_{ass} (Fig. 4). One can clearly identify a minimum in Fig. 4, which should correspond to the highest ionic conductivity, at a hypothetical atomic number between 61 (Pm) and 62 (Sm). The minimum E_a is obtained when E_f is approximately independent of the local atomic configuration, as a result of the optimal balance between elastic and electronic interactions. Our calculated E_a can be directly compared to experimental values for Y^{3+}, Nd^{3+}, Gd^{3+}, and La^{3+}, referring to the same doping concentration as the theoretical estimates (9). The experimental values are all slightly higher than our theoretical estimates, which may be related to deviations from the assumption of randomly distributed dopants. Such a deviation is supported by the calculated positive binding energies of trivalent dopants, and it would increase E_a. Our model predicts Pm^{3+} and Sm^{3+} to be the

best dopants of single dopants. Unfortunately, because Pm is radioactive, it is inconceivable to use it in real applications. The excellent properties of Sm^{3+} have been confirmed in experimental studies (23). The most important point, however, is that according to the general picture presented here, a mixture of dopants, one or both of which do not provide low E_a, may result in a good balance between the elastic and electronic contributions and therefore improve the ionic conductivity. It is obvious that for the lanthanide series, the combinations of 3+ dopants producing an average atomic number between 61 and 62 should be the right choice. We tested two possible combinations, Nd/Sm and Pr/Gd (Fig. 4). It is especially remarkable that a mixture of 3+ ions may lead to an ionic conductivity that is higher than the ionic conductivity if any of them is used as a single dopant.

To summarize, we have quantitatively predicted the connection between defect association and ionic conductivity directly from quantum mechanical calculations. Further, we have shown that a low association energy, and hence high ionic conductivity, is related to materials with an optimal balance between elastic and electronic defect interactions. We have shown how the search for better dopant combinations can be essentially narrowed in a simple and physically transparent way.

Methods

For the density functional theory calculations, we used the *ab initio* total-energy and molecular-dynamics program VASP (Vienna *ab initio* simulation program) (16, 17) with projector augmented wave (PAW) potentials (24). In this program, the wave functions are expanded in a plane-wave basis set. The exchange-correlation effects were described within the generalized gradient approximation (25). The CeO_2 host was modeled within the valence band model (26, 27), which considers 4*f* electrons of Ce as a part of the valence band. All trivalent lanthanide dopants were described by treating localized 4*f* electrons as a part of the frozen core. As previously mentioned, we modeled defect properties within $2 \times 2 \times 2$ and $3 \times 2 \times 2$ supercells, derived from the ideal fluorite structure (Fig. 1*a*). As the low defect concentration limit was addressed, we assumed the volume of the supercells to be constant and equal to the calculated volume of bulk ceria ($a = 5.469$ Å). This assumption was justified by test calculations, which showed that volume relaxation only has a minor effect on the defect parameters of present interest. We relaxed all internal structural parameters so that the Hellman–Feyman forces on each ion were negligible (<0.02 eV/Å) and the total energy was converged to at least the desired accuracy of ≈ 10 meV per cell. To assure accurate results, we used the plane-wave cut-off energy of 400 eV and a $3 \times 3 \times 3$ ($2 \times 2 \times 2$ supercell) or a $2 \times 3 \times 3$ ($3 \times 2 \times 2$ supercell) Monkhorst–Pack *k* point mesh (28). Further, Gaussian smearing with a smearing parameter of 0.20 eV was applied. We obtained the migration barriers for oxygen-vacancy diffusion by calculating the energy for oxygen in the saddle point positions. These positions were taken halfway between the oxygen sites involved in the diffusion process; however, we applied no restriction on the position in directions perpendicular to the migration path. Tests showed that the true saddle point was indeed close to the halfway position and the error introduced by the above assumption was small (≈ 0.01 eV).

We would like to thank the Swedish Research Council (VR), the Swedish Foundation for Strategic Research (SSF), and the Swedish Energy Agency (STEM) for support. Additionally, we thank the Swedish National Infrastructure for Computing (SNIC) for computing resources.

1. Inaba, H. & Tagawa, H. (1996) *Solid State Ionics* **83,** 1–16.
2. Steele, B. C. H. & Heinzel, A. (2001) *Nature* **414,** 345–352.
3. Hibino, T., Hashimoto, A., Inoue, T., Tokuno, J.-I., Yoshida, S.-I. & Sano, M. (2000) *Science* **288,** 2031–2033.
4. Park, S., Vohs, J. M. & Gorte, R. J. (2000) *Nature* **404,** 265–266.
5. Kharton, V. V., Marques, F. M. B. & Atkinson A. (2004) *Solid State Ionics* **174,** 135–149.
6. Kim, D. J. (1989) *J. Am. Ceram. Soc.* **72,** 1415–1421.
7. Kilner, J. (1983) *Solid State Ionics* **8,** 201–207.
8. Kilner, J. & Brook, R. J. (1983) *Solid State Ionics* **6,** 237–252.
9. Faber, J., Geoffroy, C., Roux, A., Sylvestre, A. & Abélard, P. (1989) *Appl. Phys. A* **49,** 225–232.
10. Gerhardt-Anderson, R. & Nowick, A. S. (1981) *Solid State Ionics* **5,** 547–550.
11. Wang, D. Y., Park, D. S., Griffith, J. & Nowick, A. S. (1981) *Solid State Ionics* **2,** 95–105.
12. Butler, V., Catlow, C. R. A., Fender, B. E. F. & Harding, J. H. (1983) *Solid State Ionics* **8,** 109–113.
13. Balducci, G., Kaspar, J., Fornasiero, P. & Graziani, M. (2000) *Chem. Mater.* **12,** 677–681.
14. Minervini, L., Zacate, M. O. & Grimes, R. W. (1999) *Solid State Ionics* **116,** 339–349.
15. Yoshida, H., Inagaki, T., Miura, K., Inaba, M. & Ogumi, Z. (2003) *Solid State Ionics* **160,** 109–116.
16. Kresse, G. & Furthmüller, J. (1996) *Phys. Rev. B* **54,** 11169–11186.
17. Kresse, G. & Joubert, J. (1999) *Phys. Rev. B* **59,** 1758–1775.
18. Yamazaki, S., Matsui, T., Ohashi, T. & Arita, Y. (2000) *Solid State Ionics* **136–137,** 913–920.
19. Bogicevic, A. & Wolverton, C. (2003) *Phys. Rev. B* **67,** 024106.
20. Krishnamurthy, R., Yoon, Y.-G., Srolovitz, D. J. & Car, R. (2004) *J. Am. Ceram. Soc.* **87,** 1821–1830.
21. Gschneider, K. A., Jr. (1985) *J. Less Common Metals* **114,** 29–42.
22. Berry, R. S., Rice, S. A. & Ross, J. (2000) *Physical Chemistry* (Oxford Univ. Press, Oxford), pp. 512–513.
23. Eguchi, K., Setoguchi, T., Inoue, T. & Arai, H. (1992) *Solid State Ionics* **52,** 165–172.
24. Blöchl, P. E. (1994) *Phys. Rev. B* **50,** 17953–17979.
25. Perdew, J. P., Chevary, J. A., Vosko, S. H., Jackson, K. A., Pederson, M. R., Singh, D. J. & Fiolhais, C. (1992) *Phys. Rev. B* **46,** 6671–6687.
26. Skorodumova, N. V., Simak, S. I., Lundqvist, B. I., Abrikosov, I. A. & Johansson, B. (2002) *Phys. Rev. Lett.* **89,** 166601.
27. Skorodumova, N. V., Ahuja, R., Simak, S. I., Abrikosov, I. A., Johansson, B. & Lundqvist, B. I. (2001) *Phys. Rev. B* **64,** 115108.
28. Monkhorst, H. J. & Pack, J. D. (1976) *Phys. Rev. B* **13,** 5188–5192.